Modeling dislocation cores in $SrTiO_3$ using the Peierls-Nabarro model

Denise Ferré, Philippe Carrez, and Patrick Cordier*
Laboratoire de Structure et Propriétés de l'Etat Solide–UMR CNRS 8008, Université des Sciences et Technologies de Lille, Cité Scientifique, Bâtiment C6, 59655 Villeneuve d'Ascq, France

(Received 16 April 2007; revised manuscript received 12 July 2007; published 23 January 2008)

We have recently determined dislocation core structures in complex minerals relevant to the Earth's mantle using the Peierls-Nabarro model. In this approach, the original Peierls-Nabarro model is coupled with first-principles calculations of generalized stacking fault. In order to test the reliability of such calculations, we study here the dislocation core properties in a perovskite-structured material, $SrTiO_3$, for which a lot of experimental information are available. Four different slip systems have been investigated in $SrTiO_3$: $\langle 100\rangle\{010\}$, $\langle 100\rangle\{011\}$, $\langle 110\rangle\{001\}$, and $\langle 110\rangle\{1\bar{1}0\}$. $\langle 110\rangle\{1\bar{1}0\}$ exhibits the lower lattice friction due to core spreading, and the next easiest slip system is found to be $\langle 100\rangle\{010\}$. It is shown that our results (dislocation core spreading and Peierls stress values) are in perfect agreement with experiments (transmission electron microscopy model of core structure and mechanical properties), providing an interesting validation of the Peierls-Nabarro model on complex materials.

DOI: 10.1103/PhysRevB.77.014106 PACS number(s): 62.20.−x

I. INTRODUCTION

A large number of materials that have paramount applications in both mineralogy and materials science exhibit a perovskite structure. In mineralogy, the lower mantle is thought to be mostly constituted by $(Mg,Fe)SiO_3$ perovskite and to a less extent by $CaSiO_3$ perovskite.[1] The dynamics of the Earth is thus largely controlled by the deformation mechanisms in perovskites. In materials science, perovskites have manifold applications for their ferroelectric, dielectric, or piezoelectric properties, for energy storage, catalysis, etc. Dislocations are important in many of these applications as an agent of deformation or in relation to their electronic properties.

Strontium titanate ($SrTiO_3$) exhibits a cubic symmetry (space group $Pm3m$; $a=3.905$ Å) and is commonly regarded as the archetypal cubic perovskite. $SrTiO_3$ has a very large dielectric constant. It is also widely used as a substrate for the epitaxial growth of high-temperature superconducting (and many oxides) thin films, for special optical windows, and as high quality sputtering target. For these reasons, several studies have addressed recently the issue of plastic deformation and dislocation properties in $SrTiO_3$. As generally observed in perovskites,[2] the most common slip systems observed in deformed $SrTiO_3$ are $\langle 110\rangle\{1\bar{1}0\}$ and $\langle 100\rangle\{010\}$.[3–6] It is, however, possible, following elaboration, to find other dislocation types such as $\langle 1\bar{1}0\rangle\{001\}$[7] or $\langle 001\rangle\{1\bar{1}0\}$.[8] The plasticity of $SrTiO_3$ exhibits a very surprising evolution with temperature with a very strong flow stress anomaly eventually leading to an inverse brittle-ductile transition.[5,6] Such behavior suggests that dislocations may exhibit several core structures. There have been several observations suggesting that some dislocations are dissociated in $SrTiO_3$, either in the glide or in the climb mode.[7,4,9,10] The core structure of dislocations in $SrTiO_3$ has been recently the subject of very detailed studies using high-resolution transmission electron microscopy (HRTEM)[8] or electron-energy-loss spectroscopy (EELS)[9,10] leading to atomic-scale models of dislocation cores. The goal of the present study is to provide numerical models of dislocations in $SrTiO_3$ to be compared with available observations.

As recently summarized by Schoeck,[11] information about the atomic arrangement around a dislocation core can be obtained in two ways, either by direct atomistic simulation or by the Peierls-Nabarro (PN) model. It is commonly recognized that the drawback of atomistic simulations is that they rely on interatomic potentials often imprecisely defined. On the contrary, the possibility to obtain accurate interplanar atomic interaction potentials through the generalized stacking fault (GSF) concept by *ab initio* calculation has led to a revival of the determination of dislocation core in a complex structure with the help of the PN model. In this study, we propose to model dislocation cores in $SrTiO_3$ with the PN model.

II. PEIERLS-NABARRO MODEL

The original PN model[12,13] represents a useful and efficient approach to calculate the core properties of dislocations[14–16] based on the assumption of a planar core.[17] It has been shown to apply to a wide range of materials.[16,18–25] The purpose of this section is to briefly review the relevant aspects of the PN model for application to dislocations in $SrTiO_3$.

The PN model assumes that the misfit region of inelastic displacement is restricted to the glide plane, whereas linear elasticity applies far from it. A dislocation is treated as a continuous distribution of shear $S(x)$ or of infinitesimal dislocations with density $\rho(x)$ (for which the total summation is equal to the Burgers vector $\mathbf{b}$) along the glide plane (x is the coordinate along the displacement direction of the dislocation in the glide plane). The restoring force F acting between atoms on either sides of the interface is balanced by the resultant stress of the distribution leading to the well-known PN equation,

$$\frac{K}{2\pi}\int_{-\infty}^{+\infty}\frac{1}{x-x'}\left[\frac{dS(x')}{dx'}\right]dx' = \frac{K}{2\pi}\int_{-\infty}^{+\infty}\frac{\rho(x')}{x-x'}dx' = F[S(x)], \tag{1}$$

where K, the energy coefficient, is a function of the dislocation character θ. The main effect of elastic anisotropy on the

dislocation line energy is found in the energy coefficient K, which can be calculated within the frame of the Stroh theory.[26] As largely developed in numerous studies since Vitek,[27,28] the solution of the PN equation can be numerically found by introducing a restoring force simply defined as the gradient of the so-called generalized stacking fault γ,

$$\vec{F}(S) = -\vec{\text{grad}}\ \gamma(S). \tag{2}$$

In the following, we determine from first principles the GSF for potential slip systems of the $SrTiO_3$ perovskite, and then we use the GSF results as an input into the PN model. Following the methodology proposed by Joos *et al.*,[29] the disregistry function S is determined by solving the PN equation with a solution in the following form:

$$S(x) = \frac{b}{2} + \frac{b}{\pi}\sum_{i=1}^{N} \alpha_i \arctan\frac{x - x_i}{c_i}, \tag{3}$$

where α_i, x_i, and c_i are variational constants. Using the previous disregistry function [Eq. (3)] in the left-hand side of the PN equation gives a trial restoring force (containing the α_i, x_i, and c_i parameters). The variational constants α_i, x_i, and c_i are fitted from a least squares minimization of the difference between the trial force and the restoring force F derived from our *ab initio* calculations (see Carrez *et al.*[23] for the details of the calculations).

In order to obtain the misfit energy corresponding to the Peierls dislocation and to determine the Peierls stress, the sum of the local misfit energy has to be done at the position of atom rows parallel to the dislocation line.[26,30] The misfit energy can thus be written as[29,15]

$$W(u) = \sum_{m=-\infty}^{+\infty} \gamma[S(ma' - u)]a', \tag{4}$$

where a' is the periodicity of W, taken as the shortest unit cell parameter in the direction of the dislocation's displacement. The Peierls stress is then given by

$$\sigma_P = \max\left\{\frac{1}{b}\frac{dW(u)}{du}\right\}. \tag{5}$$

III. COMPUTATIONAL DETAILS

First-principles calculations have been performed based on the density functional theory within the generalized gradient approximation (GGA).[31] Calculations were performed using the VASP code[32–35] and the all-electron projector-augmented-wave method.[36,37] The outmost core radius for the Sr, Ti, and O atoms are 2.5, 2.3, and 1.52 a.u. respectively. Namely, with the pseudopotentials used in this study, $4s$, $4p$ states for Sr and $3s$, $3p$ states for Ti are treated as valence states. In the simulation, the electronic density is expanded on a plane wave basis set with a single cutoff energy of 500 eV to obtain a convergence of 0.05 eV on the total energy.

Bulk properties of $SrTiO_3$ were determined by simulations using a supercell based on a $2a \times 2a \times 2a$ unit cell. Throughout this study, the first Brillouin zone was sampled using a Monkhorst-Pack grid[38] adapted for each supercell geometry.

TABLE I. Lattice parameter and elastic constants calculated *ab initio* for $SrTiO_3$ in the present study using the GGA approximation. A comparison is provided with previous calculations from Piskunov *et al.* (Ref. 39) performed with an optimized basis set. Bulk modulus B, shear modulus μ, and the Poisson ratio υ are calculated using the standard relations $B=(C_{11}+2C_{12})/3$, $\mu=C_{44}$, and $\upsilon=C_{12}/(C_{11}+C_{12})$.

	a (Å)	C_{11} (GPa)	C_{12} (GPa)	C_{44} (GPa)	B (GPa)	υ	$\mu/(1-\upsilon)$ (GPa)
This work	3.939	319.9	99.4	109.3	173	0.237	143.3
Piskunov *et al.* (PWGGA)	3.95	312.9	98.0	113.4	170	0.238	154.9

The crystallographic structure of $SrTiO_3$ was optimized (full relaxation of cell parameters and of atomic positions) using an $8\times8\times8$ **k**-point mesh, and the athermal elastic constant were determined as the second order derivative of the energy of a strained equilibrium cell. Results of cell parameter and elastic constant presented in Table I are in fairly good agreement with available data from recent theoretical work or experimental values (e.g., Piskunov *et al.*[39] or Cappellini *et al.*[40] and references herein). As commonly noticed, the discrepancy between values comes mostly from the choice of first-principles approximations.

Calculating a GSF for a given slip system requires a supercell with a geometry adapted to the shear plane and direction. Among several possibilities,[41] we have chosen to build supercells on a Cartesian reference frame defined by the normal of the stacking fault plane and by the shear direction. A vacuum buffer is added in the direction normal to the slip plane to avoid interaction between repeated stacking faults resulting from the use of periodic boundary conditions. Thus, for all the GSF calculations, three distinct supercells were used (Fig. 1). The number of atoms was limited to 30 atoms per supercell. The GSF excess energies γ are finally calculated by imposing a given shear displacement value to the upper part of the supercell. All atoms but those located close to the buffer layer are allowed to relax in the directions perpendicular to the shear direction in order to minimize the energy of the GSF. Further details of the supercell construction and relaxation conditions can be found elsewhere.[42]

IV. RESULTS

A. Generalized stacking faults

The result of the four GSF calculations are presented in Fig. 2. The Burgers vector lengths are taken as 3.939 and 5.571 Å for $\langle 100\rangle$ and $\langle 110\rangle$, respectively. All the GSFs exhibit a single peak shape that can be significantly different from a cosine profile, particularly for the case of $\langle 110\rangle\{1\bar{1}0\}$, which is characterized by a plateau around $\gamma^{\max}$. This slip system is also characterized by the lowest energy

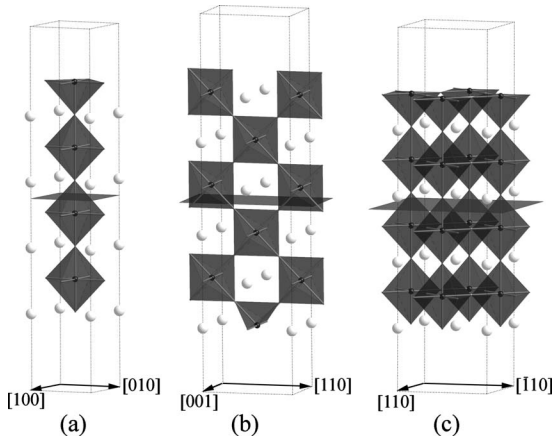

FIG. 1. Supercells used in this study to calculate the GSFs. For all the supercells, light gray spheres correspond to Sr atoms; oxygen octahedra are displayed in gray with a small black sphere in the center corresponding to the Ti atom. The shear plane located in the middle of the supercell is represented in gray. (a) Supercell used for [100](001), (b) supercell used for [001](1$\bar{1}$0) and [110](1$\bar{1}$0), and (c) supercell used for [110](001). For all the supercells, atoms present on outer surface layers are kept fixed during the GSF calculation to mimic the action of a surrounding bulk material.

value (Table II), and strong differences are found between the shear resistances along ⟨110⟩ on the {1$\bar{1}$0} or on the {100} planes. These differences are also revealed by the value of the ideal shear stress (or τ^{max}) defined as the maximum value of the restoring force F (i.e., the maximum slope of the GSF). One can see in Table II that three slip systems (⟨100⟩{010}, ⟨100⟩{011}, and ⟨110⟩{001}) exhibit comparable τ^{max}, whereas ⟨110⟩{1$\bar{1}$0} appears to have the lowest ideal shear stress.

B. Dislocation cores and Peierls stresses

Once the restoring force F is determined through the *ab initio* calculation of the GSF, one can calculate the size of the dislocation core by solving the PN equation. The order N of the disregistry function S [Eq. (3)] was adjusted to $N=6$

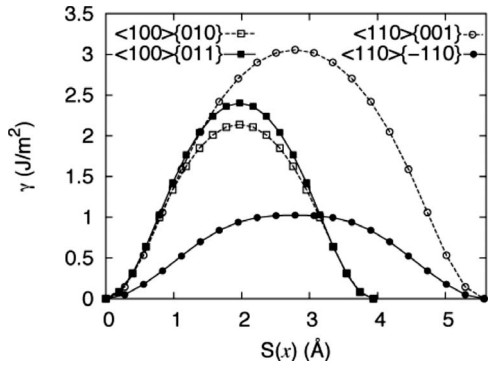

FIG. 2. Generalized stacking faults (GSFs) calculated in this study. The GSF are plotted against the shear displacement vector $S(x)$.

TABLE II. Parameters obtained from the GSF calculations. γ^{max} is the maximum value of the excess energy barrier. τ^{max} is the ideal shear stress. In the last column, τ^{max} is normalized by the shear modulus μ.

Slip system	γ^{max} (J/m^2)	τ^{max} (GPa)	τ^{max}/μ
⟨100⟩{010}	2.14	18.1	0.16
⟨100⟩{011}	2.40	20.2	0.18
⟨110⟩{001}	3.05	19.0	0.17
⟨110⟩{110}	1.02	6.7	0.06

for the four slip systems. Using symmetrical consideration, the dislocation density can be viewed as the sum of two terms (as represented in Fig. 3) that contribute to the total density. The value of K used in the PN equation was determined considering $SrTiO_3$ as an anisotropic crystal and are presented in Tables III and IV. These values can be compared to isotropic shear modulus and Poisson ratio presented in Table I, showing that $SrTiO_3$ is very close to an isotropic material.

The dislocation densities ρ determined in this study are presented in Fig. 3 for screw characters (edge characters are very similar, although systematically wider). All the cores are relatively wide with an extension over at least one periodicity. ⟨110⟩{1$\bar{1}$0} dislocations show a tendency toward dissociation although the partial dislocations are strongly overlapping.

The solution of the PN model is used to build atomistic models of the dislocation cores. We start from a perfect crystal. Following the Peierls approach, the crystal is bisected into two parts above and below the glide plane. The atomic rows of the upper part are shifted according to the shear profile $S(x)$ calculated in the PN model. The final shape of the lattice planes is obtained by adding the isotropic elastic displacement field associated with the dislocation (of density ρ). Figure 4 presents atomistic models for the four types of dislocations considered in the present study.

Finally, the misfit energy $W(u)$ and the Peierls stresses were determined using Eqs. (4) and (5). An example of $W(u)$ is presented in Fig. 5 for a ⟨100⟩{010} edge dislocation. The four slip systems exhibit significantly different Peierls stresses (see Tables III and IV). ⟨110⟩{1$\bar{1}$0} appears to be the easiest slip system with Peierls stresses of the order of a few megapascals. On the opposite side, ⟨100⟩{011} is the hardest slip system with plastic deformation controlled by Peierls friction on the screw segments (of ~10 GPa). In between, we find ⟨100⟩{010} and ⟨110⟩{001} with Peierls stresses around 1 GPa.

V. DISCUSSION

The study of the GSF provides the first information about the ability of the $SrTiO_3$ perovskite to undergo plastic shear. One can see readily in Fig. 2 that shear along ⟨110⟩{1$\bar{1}$0} is significantly easier than along the three other slip planes con-

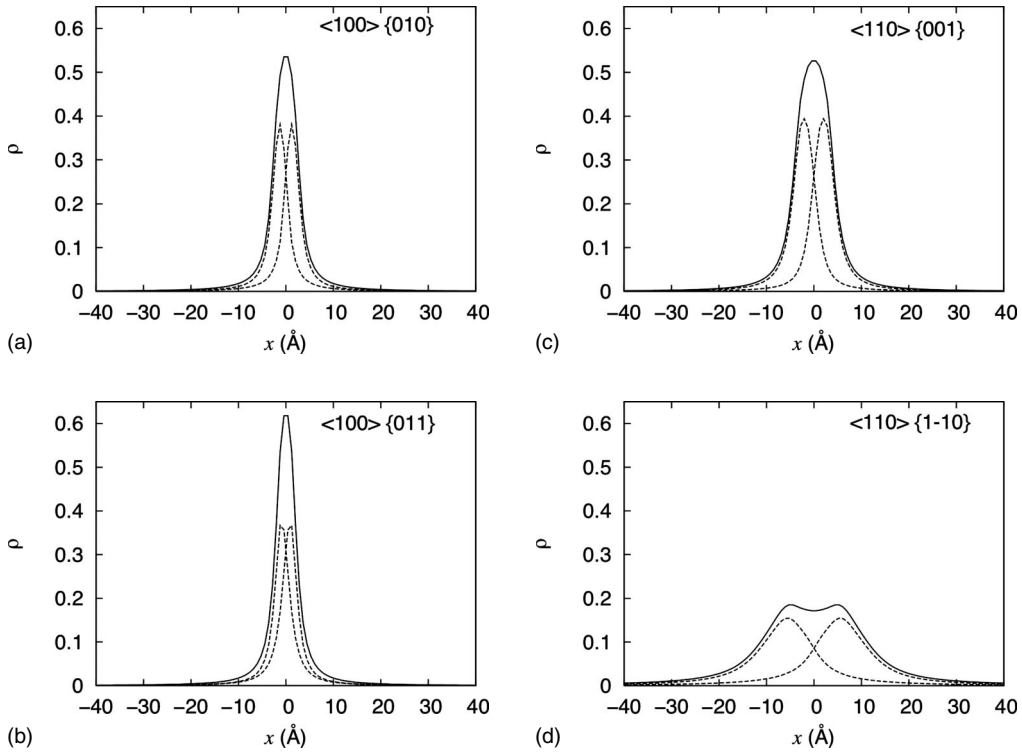

FIG. 3. Dislocation density (ρ) for screw dislocations in the $SrTiO_3$ perovskite calculated for the following slip systems: (a) $\langle 100\rangle\{010\}$, (b) $\langle 100\rangle\{011\}$, (c) $\langle 110\rangle\{001\}$, and (d) $\langle 110\rangle\{1\bar{1}0\}$.

sidered. The PN model provides, however, a more elaborate level of understanding as it gives information about the dislocation core fine structure. In particular, the PN model gives information about the tendency of the core to spread along the glide plane. Core spreading has a profound influence on the lattice friction borne by the dislocation and hence on its mobility. Figure 3 emphasizes the picture drawn from the GSF. One can see that $\langle 100\rangle\{010\}$, $\langle 100\rangle\{011\}$, and $\langle 110\rangle\{001\}$ dislocations exhibit no splitting, although their distributions can be mathematically decomposed into two strongly overlapping partial dislocations. The situation is different for $\langle 110\rangle\{1\bar{1}0\}$ dislocations. The plateau observed on the GSF results in a significant core spreading. Partial dislocations are not individualized, however. The implications of these core structures can be appraised from Tables III and IV, which show that $\langle 110\rangle\{1\bar{1}0\}$ dislocations bear much lower Peierls frictions than the other dislocations.

Given the strong sensitivity of Peierls friction to dislocation core spreading, one can question the reliability of the Peierls model to reproduce dislocation core profiles in com-

TABLE III. Results of the Peierls-Nabarro model for screw dislocations. a' is the periodicity of the Peierls valley. ζ is the half-width of the dislocation core deduced from the numerical solution of the PN equation. Δ is the partial dislocation separation distance. ζ and Δ are given in Å and also as a function of a' in brackets. ΔW corresponds to the Peierls energy barrier, and σ_p is the calculated Peierls stress needed to overcome the energy barrier.

Slip system	$K(0)$ (GPa)	a' (Å)	ζ (Å)	Δ (Å)	ΔW (10^{-11} J/m)	σ_p (GPa)
$\langle 100\rangle\{010\}$	110.00	3.939	2.830 (0.72)		3.20	0.7
$\langle 100\rangle\{011\}$	110.00	5.571	2.308 (0.41)		65.70	9.9
$\langle 110\rangle\{001\}$	109.25	5.571	4.320 (0.77)		7.76	0.9
$\langle 110\rangle\{110\}$	109.25	3.939	11.767 (2.99)	9.898 (2.51)	0.04	0.006

TABLE IV. Results of the Peierls-Nabarro model for edge dislocations. a' is the periodicity of the Peierls valley. ζ is the half-width of the dislocation core deduced from the numerical solution of the PN equation. Δ is the partial dislocation separation distance. ζ and Δ are given in Å and also as a function of a' in brackets. ΔW corresponds to the Peierls energy barrier, and σ_p is the calculated Peierls stress needed to overcome the energy barrier.

Slip system	$K(90)$ (GPa)	a' (Å)	ζ (Å)	Δ (Å)	ΔW (10^{-11} J/m)	σ_p (GPa)
$\langle 100\rangle\{010\}$	143.94	3.939	3.686 (0.93)		2.90	0.6
$\langle 100\rangle\{011\}$	143.99	3.939	3.019 (0.77)		2.88	0.6
$\langle 110\rangle\{001\}$	144.49	5.571	5.697 (1.02)		11.50	1.2
$\langle 110\rangle\{110\}$	144.07	5.571	15.497 (2.78)	13.188 (2.37)	0.04	0.004

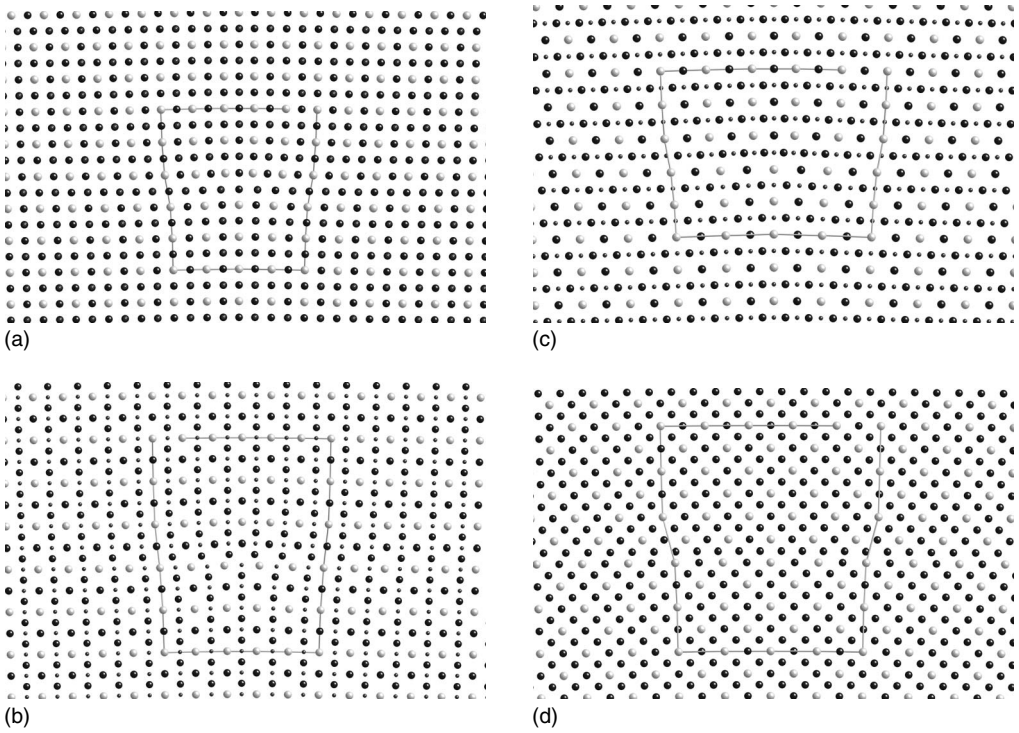

FIG. 4. Atomistic models for edge dislocations in the $SrTiO_3$ perovskite calculated for the following slip systems: (a) ⟨100⟩{010}, (b) ⟨100⟩{011}, (c) ⟨110⟩{001}, and (d) ⟨110⟩{1$\bar{1}$0}. For the four structures, light gray spheres correspond to Sr, small black spheres to Ti, and large black spheres to O.

plex materials. $SrTiO_3$ represents an excellent test material as recent studies have provided HRTEM micrographs of dislocation cores of very high quality. Indeed, Jia *et al.*[8] showed that a combination of hardware correction of the spherical aberration with numerical phase-retrieval techniques could capture detailed atomic arrangements of cations and anions in the dislocation core of a ⟨100⟩{011} dislocation in $SrTiO_3$. Their study [reproduced in Fig. 6(a) with permission] provides a direct counterpart to our numerical models. Figure 6(c) demonstrates that the size of the dislocation is perfectly reproduced by the Peierls model. A further comparison can be made with the study of Zhang *et al.*,[9] who inferred possible models for ⟨100⟩{010} dislocations (in a symmetrical tilt boundary) from HRTEM and EELS. In Fig. 6 of their paper, Zhang *et al.*[10] proposed four possible dislocation core models (labeled A, B, C, and D) for ⟨100⟩{010} dislocations, which correspond to different cut levels for the glide plane and different core terminations (SrO or TiO). They show that only core models labeled B and C can match the EELS data. Our study shows that these B and C core models correspond to the same core structure represented at different positions in the glide plane along the glide direction. Indeed, considering the Peierls potential associated with the motion of ⟨100⟩{010} edge dislocations (Fig. 5), two distinct core structures can be considered: one, stable, characterized by the lowest misfit energy (i.e., in the Peierls valley) and another one, unstable, corresponding to the highest misfit energy (i.e., on top of the Peierls hill). We find that case B corresponds to the valley position, whereas case C corresponds to the top-hill position. Therefore, we suggest that the dislocation studied by Zhang *et al.* must correspond to their B model [which corresponds to the model depicted in Fig. 4(a)].

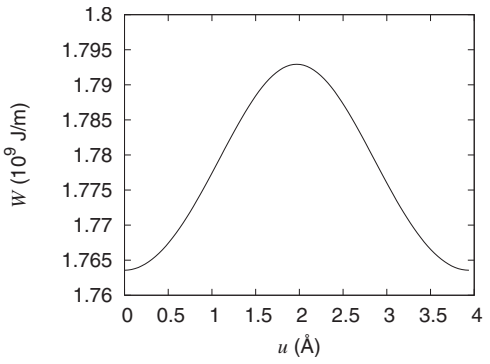

FIG. 5. Misfit energy W for a ⟨100⟩{010} edge dislocation, plotted as a function of the position u of the dislocation core. As noted by Joos *et al.* (Ref. 29), the average misfit energy for all positions of the dislocation corresponds to the classical energy of a dislocation $Kb^2/4\pi$.

What do we learn about the plasticity of the $SrTiO_3$ perovskite from dislocation core modeling? There seems to be a general trend that perovskites slip on ⟨110⟩{1$\bar{1}$0} at low temperature with an increasing activity of ⟨100⟩{010} (involving climb?) at higher temperature.[2] $SrTiO_3$ perovskite follows this trend.[3,4,43] The temperature dependence of plastic deformation of the $SrTiO_3$ perovskite has been investigated over a large range (from liquid nitrogen to 1800 K) on single crystals oriented to activate ⟨110⟩{1$\bar{1}$0} slip.[5,6] Discussing these

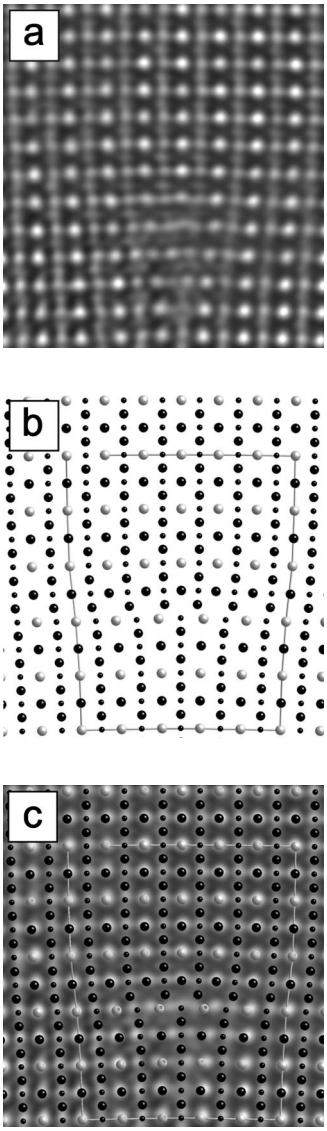

FIG. 6. Comparison of the PN model for a ⟨100⟩{011} edge dislocation with experiments. a) Experimental TEM micrograph of Jia *et al.* (Ref. 8) reproduced with permission. (b) Calculated ⟨100⟩{011} edge dislocation core structure from the PN model. (c) Calculated structure superimposed on the experimental image for comparison.

results, Zhang *et al.*[10] observed that "the temperature dependence of the critical resolved shear stress of ⟨110⟩{1$\bar{1}$0} dislocations is weak (comparable to that of many fcc metals), even down to liquid-nitrogen temperature." This is in excellent agreement with the Peierls stresses found in this study (see Tables III and IV). The (slightly dissociated) core structure depicted in Fig. 4(d) is likely to describe ⟨110⟩{1$\bar{1}$0} dislocations in the low-temperature regime. At temperatures above ~900 K, the critical flow stress for ⟨110⟩{1$\bar{1}$0} slip increases (for either ⟨110⟩ or ⟨100⟩ oriented samples). This has led Gumbsch *et al.*[6] to propose that ⟨110⟩{1$\bar{1}$0} dislocations could exhibit a "high-temperature" core structure, more difficult to move than the one depicted in Fig. 4(d). There exist many possibilities to account for such behavior. One, analogous to the case of bcc metals, could be that screw dislocations adopt a three dimensional structure. Our calculations based on the PN model cannot calculate such structures, but we note that (contrary to some cases identified in previous studies[24,25]) we do not find that ⟨110⟩ dislocations tend to spread in several planes simultaneously. Although not representing a final argument, this does not support the hypothesis of a three dimensional core. Another possibility is that dislocations exhibit dissociation in the climb mode. This possibility has been put forward earlier by Mao and Knowles[7] based on TEM observations and has recently been confirmed by Zhang *et al.*[10] using HRTEM and EELS. The dislocations are dissociated following the collinear reaction $\langle 110\rangle = 1/2\langle 110\rangle + 1/2\langle 110\rangle$, with the partial dislocations being separated by a stacking fault on a nonslip plane. Zhang *et al.*[10] showed that this climb dissociation could be further stabilized if the core is oxygen deficient. Climb dissociation at high temperature must result in a severe decrease of the mobility of ⟨110⟩ dislocations. This can explain the flow stress anomaly reported[5,6] as well as the predominance of ⟨100⟩ glide reported at high temperature.[3,4,43] Concerning a ⟨100⟩ glide, our calculations confirm that easiest slip takes place on {001}, in agreement with most observations.

VI. CONCLUSION

The PN model provides information on dislocation core structures and plasticity in $SrTiO_3$. Despite the fact that ⟨110⟩ does not correspond to the smallest lattice repeat, ⟨110⟩{1$\bar{1}$0} is the easiest slip system. This is due to a tendency toward core spreading into the glide plane for this slip system. Our calculations are consistent with the high-mobility, low-temperature core structure assumed by Brunner *et al.*[5] and Gumbsch *et al.*[6] These authors have shown, however, that ⟨110⟩{1$\bar{1}$0} dislocations exhibit at high-temperature, low-mobility core structure (involving climb dissociation), which cannot be predicted within the frame of the PN model. The second slip system is ⟨100⟩{010} as usually reported (⟨100⟩{110} is, in fact, the slip system observed at high-temperature).

Our results compare well with the experimental results of Zhang *et al.*[10] (for which our calculation provides further constraint on the core structure as deduced from EELS measurements) and of Jia *et al.*[8] In the latter case, a direct comparison with experimental HRTEM micrographs validates the PN model for complex materials in determining the size of a dislocation core. This validation is important as the PN model is presently one of the rare approaches available to infer dislocation properties in one of the most important phase of the Earth's mantle: $MgSiO_3$ perovskite.

ACKNOWLEDGMENTS

Computational resources have been provided by IDRIS (Project No. 031685) and CRI-USTL supported by the Fonds Européens de Développement Régional and Région Nord–Pas de Calais. Jia is warmly thanked for having provided his experimental HRTEM micrograph.

*Corresponding author; patrick.cordier@univ-lille1.fr

[1] A. E. Ringwood, Geochim. Cosmochim. Acta **55**, 2083 (1991).
[2] J. P. Poirier, S. Beauchesne, and F. Guyot, in *Perovskite: A Structure of Great Interest to Geophysics and Materials Science*, edited by A. Navrotsky and D. Weidner (AGU, Washington, D.C., 1989), p. 119.
[3] J. Nishigaki, K. Kuroda, and H. Saka, Phys. Status Solidi A **128**, 319 (1991).
[4] T. Matsunaga and H. Saka, Philos. Mag. Lett. **80**, 597 (2000).
[5] D. Brunner, S. Taeri-Baghbadrani, W. Sigle, and M. Rühle, J. Am. Ceram. Soc. **84**, 1161 (2001).
[6] P. Gumbsch, S. Taeri-Baghbadrani, D. Brunner, W. Sigle, and M. Rühle, Phys. Rev. Lett. **87**, 085505 (2001).
[7] Z. Mao and K. M. Knowles, Philos. Mag. A **73**, 699 (1996).
[8] C. L. Jia, A. Thust, and K. Urban, Phys. Rev. Lett. **95**, 225506 (2005).
[9] Z. Zhang, W. Sigle, W. Kurtz, and M. Rühle, Phys. Rev. B **66**, 214112 (2002).
[10] Z. Zhang, W. Sigle, and M. Rühle, Phys. Rev. B **66**, 094108 (2002).
[11] G. Schoeck, Acta Mater. **54**, 4865 (2006).
[12] R. E. Peierls, Proc. Phys. Soc. London **52**, 34 (1940).
[13] F. R. N. Nabarro, Proc. Phys. Soc. London **59**, 256 (1947).
[14] Q. Ren, B. Joos, and M. S. Duesbery, Phys. Rev. B **52**, 13223 (1995).
[15] B. Joos and M. S. Duesbery, Phys. Rev. Lett. **78**, 266 (1997).
[16] J. N. Wang, Mater. Sci. Eng., A **206**, 259 (1996).
[17] G. Schoeck, Mater. Sci. Eng., A **400-401**, 7 (2005).
[18] V. V. Bulatov and E. Kaxiras, Phys. Rev. Lett. **78**, 4221 (1997).
[19] B. von Sydow, J. Hartford, and G. Wahnström, Comput. Mater. Sci. **15**, 367 (1999).
[20] G. Lu, N. Kioussis, V. V. Bulatov, and E. Kaxiras, Phys. Rev. B **62**, 3099 (2000).
[21] G. Lu, in *Handbook of Materials Modeling. Volume 1: Methods and Models*, edited by S. Yip (Springer, New York, 2005), p. 1.
[22] C. R. Miranda and S. Scandolo, Comput. Phys. Commun. **169**, 24 (2005).
[23] P. Carrez, P. Cordier, D. Mainprice, and A. Tommasi, Eur. J. Mineral. **18**, 149 (2006).
[24] P. Carrez, D. Ferré, and P. Cordier, Philos. Mag. **87**, 3229 (2007).
[25] J. Durinck, P. Carrez, and P. Cordier, Eur. J. Mineral. **19**, 631 (2007).
[26] J. P. Hirth and J. Lothe, *Theory of Dislocations* (Wiley, New York, 1982).
[27] V. Vítek, Philos. Mag. **18**, 773 (1968).
[28] J. W. Christian and V. Vitek, Rep. Prog. Phys. **33**, 307 (1970).
[29] B. Joos, Q. Ren, and M. S. Duesbery, Phys. Rev. B **50**, 5890 (1994).
[30] G. Schoeck, Philos. Mag. A **79**, 2629 (1999).
[31] J. P. Perdew and Y. Wang, Phys. Rev. B **45**, 13244 (1992).
[32] G. Kresse and J. Hafner, Phys. Rev. B **47**, 558 (1993).
[33] G. Kresse and J. Hafner, Phys. Rev. B **49**, 14251 (1994).
[34] G. Kresse and J. Furthmüller, Phys. Rev. B **54**, 11169 (1996).
[35] G. Kresse and J. Furthmüller, Comput. Mater. Sci. **6**, 15 (1996).
[36] P. E. Blöchl, Phys. Rev. B **50**, 17953 (1994).
[37] G. Kresse and D. Joubert, Phys. Rev. B **59**, 1758 (1999).
[38] J. P. Perdew and A. Zunger, Phys. Rev. B **23**, 5048 (1981).
[39] S. Piskunov, E. Heifets, R. I. Eglitis, and G. Borstel, Comput. Mater. Sci. **29**, 165 (2004).
[40] G. Cappellini, S. Bouette-Russo, B. Amadon, C. Noguera, and F. Finocchi, J. Phys.: Condens. Matter **12**, 3671 (2000).
[41] V. V. Bulatov, W. Cai, R. Baran, and K. Kang, Philos. Mag. **86**, 2847 (2006).
[42] J. Durinck, A. Legris, and P. Cordier, Am. Mineral. **90**, 1072 (2005).
[43] Z. C. Wang, S. Karato, and K. Fujino, Phys. Earth Planet. Inter. **79**, 299 (1993).